Monitoring of coal fracturing in underground coal gasification by acoustic emission techniques

Monitoring of coal fracturing in underground coal gasification by acoustic emission techniques

Faqiang Su[a,b], Ken-ichi Itakura [b,c,*], Gota Deguchi[d], and Koutarou Ohga[e]

[a] School of Energy Science and Engineering, Henan Polytechnic University, 2001 Century Avenue, Jiaozuo, Henan, 454003, China
[b] Center of Environmental Science and Disaster Mitigation for Advanced Research, Muroran Institute of Technology, 27-1 Mizumoto, Muroran 050-8585, Japan
E-Mail: sfqmuroran@gmail.com
[c] Graduate School of Engineering, Muroran Institute of Technology, 27-1 Mizumoto, Muroran 050-8585, Japan
E-mail: itakura@mmm.muroran-it.ac.jp
[d] Underground Resources Innovation Network, NPO, Higashi-ku, Sapporo 007-0847, Japan
E-Mail: gota@mue.biglobe.ne.jp
[e] Graduate School of Engineering, Hokkaido University, Kita-ku, Sapporo 060-8628, Japan
E-Mail: k-ohga@eng.hokudai.ac.jp

***** E-mail: itakura@mmm.muroran-it.ac.jp; Tel.: +81-143-46-5424; Fax: +81-143-46-5499

Abstract

During the underground coal gasification (UCG) process, fracturing and cracks occur inside the gasification zone and surrounding rocks as the underground coal cavity evolves. Although fracturing activity and crack extension directly affect gasification efficiency and have environmental impacts, little research to date has focused on their effects. This study discusses the application of acoustic emission (AE) analysis for the evaluation of distinctly designed UCG models and operational parameters and describes the gasification process based on its results. We studied the cavity growth, fracturing mechanism, and the effects of various design and operational variables, such as linking-hole type, gas feed rate, and gasification agent. We found that the AE activity was closely related to the temperature change occurring inside the coal, with AE generation apparently resulting from crack initiation and extension around the coal gasification area, which occurs as a result of thermal stress. UCG modeling showed that the location of AE sources reflects the size of the gasification area and the cavity growth. In addition, the quantitative information on the located AE sources can be obtained. The introduction of a process control system into UCG modeling along with AE monitoring allowed for the real-time monitoring of the fracturing and cavity evolution inside a combustion reactor. Together, these processes have the potential to significantly reduce field risk in UCG by enabling the timely adjustment of operational parameters. Thus, AE monitoring is useful for maintaining a safe and efficient UCG process.

Keywords: Acoustic emission (AE); Underground coal gasification (UCG); UCG model; Cavity growth; Crack distribution

1. Introduction

Fossil fuels remain the primary energy source worldwide, and coal, the most abundant fossil fuel source, is responsible for providing a high percentage of electricity generation. Most power plants still use combustion processes [1, 2] and are responsible for the emission of stationary-source carbon into the air. As the largest developing countries with maximal coal yield and consumption, China and India use coal as their primary energy source. In particular, considering the amount of coal in India and its high ash content (13.5%–50%), low calorific value, and seam depth, there is a distinct need to make better use of these resources [3, 4]. Increasingly serious climate and environmental problems have also spurred interest in research on the development of clean and efficient coal technologies. Underground coal gasification (UCG) is a promising environmentally acceptable technique for the utilizing coal reserves, particularly those at great depths or under complicated geological conditions that are unmineable or uneconomic with conventional production methods [5–12]. UCG involves the gasification of coal within the seam via a process of injecting oxidants through an injection well and extracting the resulting syngas through a production well. This process has only a modest environmental impact and produces an easily transportable product that can serve as fuel gas or chemical feedstock or be used for liquid fuel production [13, 14]. In some cases of deep coal seam, many UCG operations also create by-product of CO_2 suitable for developing an UCG-CCS (carbon capture and sequestration) system with the technological development of CO_2 capture and storage [5, 10, 15-18]. Hydrogen production from underground coal gasification has also been pursued in recent years [19–22]. UCG has several advantages over surface coal gasification, including cost efficiency, elimination of ash waste, and provides the potential site (cavity formed in underground) for carbon sequestration [8, 23].

The idea of UCG was first proposed by Sir William Siemens in 1868 [24] as a means of solving the problems of smoke pollution in industrial cities. Instead of burning coal at the surface, he suggested placing a conventional surface coal gasifer into a mine and gasifying waste and slack coal underground. Two decades later, Dimitri I. Mendeleev noted that gasifying coal *in situ* could potentially lower cost inputs (less equipment for excavation), improve labor safety (with no underground labor required), and allow for more convenient transportation (gas pipeline transport) than traditional mining [25, 26]. In 1910, an American engineer Anson G. Betts who were granted three patents for inventing a method of gasifying the unmined coal and considered effect of various important factors on coal gasification *in situ* [27–29]. Jolley *et al*. reported early experimental attempts to the underground coal gasification [30–32].

Owing to these significant advantages, UCG has been attempted in many countries through laboratory-scale experiments and field tests [33–43], and was even applied in the USSR for industrial scale power production [5]. Recently, there has been an increased interest in UCG study [44–48] and many noteworthy modeling investigations were developed for investigating the various effects on gasification efficiency, flame propagation, coal consumption, etc. However, the process incurs

potential risks in the form of surface gas leakage, groundwater contamination, and surface depression as a result of improper UCG operation or other unpredictable factors, as coal spalling and the evolution of the underground cavity causes changes to the target coal seam and surrounding rock layers. In the 1970s and 1980s, dozens of UCG trials were performed in the U.S.; three of these tests (Hoe Creek I, II, and III) at Hoe Creek, Wyoming [49–52] produced water contamination and subsidence that were possibly caused by over-pressurization and excess fracturing in the gasification area. Environmental risk assessments require the consideration of cracking under high cavity temperatures, cavity growth, and the fracture mechanism during and after the UCG process. There is little information available in literature about the fracturing activities with the crack initiation and extension around underground gasifier during UCG process. Therefore, a precise evaluation of the combustion area of the underground coal seam is necessary. In particular, monitoring of fracture activity in the coal seam and surrounding rock is important not only for efficient gas production but also for the estimation of subsidence, pollution of underground aquifers, and gas leakage to the surface. The creation of a combustion reactor in an underground coal seam during the UCG process involves the flow of oxygen and other gases through an injection well and the collection of heat energy and gases from a production well. As gasification progresses, the combustion reactor is moved along the linking hole. In this process, the fracturing activity inside the coal seam serves an important role in enlarging the gasification zone through a process of continuous surface area oxidization caused by coal cracking. For effective coal gasification, this fracturing activity must be controlled. Moreover, excess fractures inside the coal seam and surrounding rock can induce cavity collapse, subsidence, contamination of local freshwater aquifers, etc. Therefore, monitoring and controlling of fracturing activity in underground areas are key technological requirements for efficient and safe UCG. The main objective of this study was the assessment of the feasibility of applying a new approach i.e., acoustic emission (AE) technologies for monitoring cavity growth during the UCG process in order to determine the mechanism of AE generation and then visualize fracturing activities in the gasification zone. To this end, a series of ex-situ UCG models were constructed. During coal combustion, temperatures inside the coal, contents of the product gases (reported in literature [53]), and AE activity were successively monitored at controlled feed gas (air/oxygen and steam) flow rates. Based on this, crack distribution models were developed using AE moment tensor analysis. The obtained results can be used for the observation of fracture configuration and cracks in order to develop fundamental data to be used in technology and simulation methods for evaluating the combustion zone during UCG.

2. Material and methods

2.1. Description of the experimental setup

In this study, experimental simulation of UCG in coal block samples was conducted using ex-situ laboratory UCG models, which were used to analyze fractures occurring in the gasification zone by varying several operational parameters (linking-hole type, feed gas, operational time, etc.).

The coal samples for the UCG trials were obtained from the Kushiro and Bibai Coal Mine located in Hokkaido, Japan. This coal is bituminous and characterized by a high sulfur and relatively low moisture content [53]. The raw coal blocks were shaped into rectangular cross sections and cast in a drum can with concrete in order to simulate both the coal seam and the surrounding rock layers. The

reactor walls were made of heat-resistant concrete of a specific thickness, thus providing an internal active space.

A schematic of the gasifier structure is shown in Fig. 1. This setup consists of the simulated gasifier, a gas agent supply system, a syngas cooling plant, and a gas chromatograph for analyzing the product gas compositions at specific sampling times. The location and propagation of the gasification zone were monitored by measuring the temperature using thermocouples and by monitoring fracture using AE sensors equipped within the models.

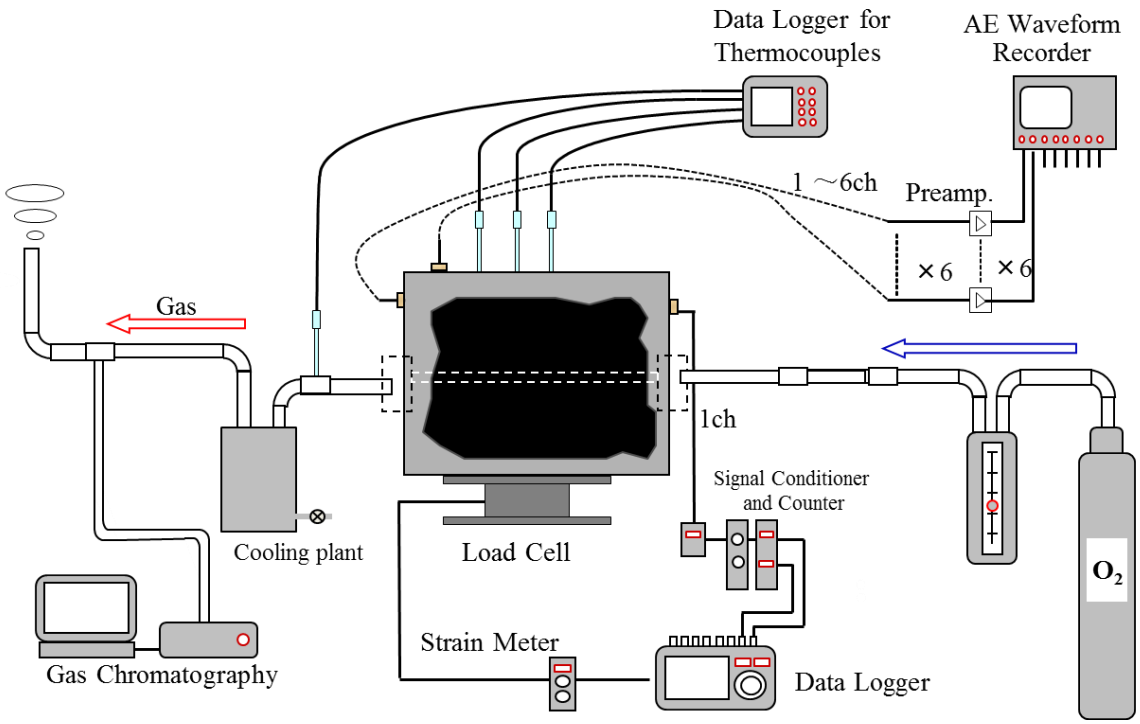

Fig. 1. Schematic of ex-situ experimental setup.

In a typical UCG process, two vertical wells are drilled into the coal seam and designed for the injection and production, connected by an underground gasification gallery created using various linking techniques at some distance apart. However, it is difficult to employ a universal design of UCG system directly to a target underground coal seam which is buried in a complex geological structure or need to consider the ground conditions. An underground reactor is created in an UCG system, which expands around the gasification channel. The underground-link, i.e., gasification channel between two wells needs to be established in the target coal seam as the underground primitive conditions, surrounding rock characteristics, and coal properties cannot readily provide a porous gasification channel for the gas flow and continuation of gasification process. Moreover, the geometry and dimensions of the experimental model seem to affect the product gas parameters and gasification efficiency. In this study, three link methods, namely, V-shaped and L-shaped linking-holes and Coaxial-hole UCG models were designed and conducted.

The sections and dimensions of the typical simulated L-shaped (L), V-shaped (V) linking-hole models, and Coaxial-hole models (C1 and C2) used in this study are shown in Fig. 2. In each model, an irregular rectangular coal block was cast in the drum can (φ 27.5 × 36 cm) with heat-resistant concrete. As shown in the figure, the linking holes set in the models for supplying the reactant gas, extracting

production gases, and also worked as the gasification channel. Wherein, the 22-mm-diameter injection hole of the L-shaped model was drilled for convenient ignition and injecting the reactant gas. As shown in Fig. 2 (b), the V-shaped 13 × 13 mm linking-hole was prepared for injection and production. In the coaxial-hole UCG model (C1 and C2), a thin inner pipe used for the injection of oxidant is located within an outer pipe that serves as a gas production outlet. To adjust the outlet position, the inner pipe is slid up and down. And the distinct type of reactant gas (pure oxygen/C1, and gas mixture of air and oxygen/C2) is employed in these two experiments. The figure also shows the locations of the thermocouples and the AE sensor arrangement. The positions of the thermocouples mounted inside the models are denoted as "channel (CH)" as shown in the figure.

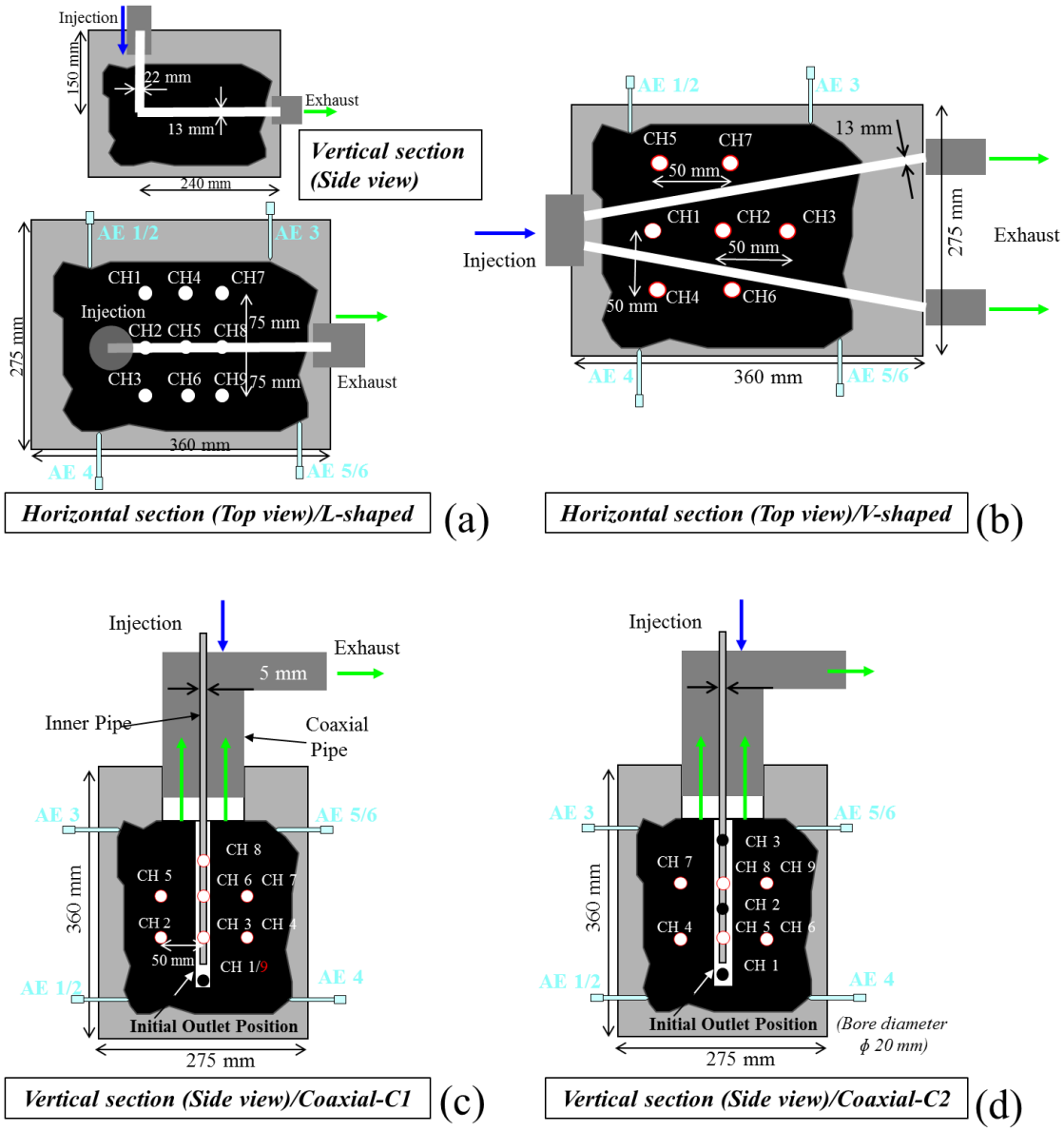

Fig. 2. ~~Vertical~~ Cross-sections and deployment of acoustic emission (AE) sensors/thermocouples in ex-situ reactors. ((a): Horizontal cross-section of L-shaped linking-hole model, (b): Horizontal cross-section of V-shaped linking-hole model, (c/d): Vertical cross-sections of Coaxial-hole models C1/C2; "CH" denotes channel of thermocouple.)

2.2. Process control and AE monitoring

In this study, pure oxygen derived from a feeding gas system consisting of a high-pressure oxygen cylinder, a steam-generating plant, and a flow rate controller was used as the gasification agent. To initiate combustion, a gas burner was passed through the injection hole. The ignition process lasted a short period of time (5–10 min). After confirmation that the coal block had ignited in the designed position, pure oxygen was continuously supplied to the gasifier for the remaining time of the experiment, which was terminated when the fire front reached the coal block border by stopping the oxygen supply, leading to a quick combustion halt and a suppression of gasification.

To measure the gasification cavity evolution and the temperature changes inside the reactor, the thermocouples were placed at depths just touching the coal block surface, i.e., at the border between the coal block and the heat-resistant concrete, or directly next to the gasification channel. The AE events and count rate from sensors mounted inside a coal block or pasted on the model surface were recorded using a data logger (GL900; Graphtec Corp., Yokohama, Japan), which respectively depict the frequency of AE occurrence, i.e., the amount of cracks initiated inside coal and the magnitude of an AE event. For each model, AE waveforms from sensors were recorded using a multi-recorder (GR-7000; Keyence Co., Osaka, Japan) with a sampling time of 5–10 μs. Changes in the gas composition, AE count rate and events, and the distribution of temperatures in a UCG model were measured over the course of each experiment.

3. Results and Discussion

Principal results in terms of product gas concentrations, gasification rates, etc. from the V, L, and C1 model experiments were discussed in our earlier work [53]. Energy recovery was also evaluated by using the proposed stoichiometric method. To optimize the UCG process and avoid potential risks, it is important to monitor the gasification process and understand the fracturing activities occurring in the coal seam, especially in the zone around the gasification cavity that is exposed by the propagation of combustion fracturing. In this study, we investigated the fracturing behavior, the cavity growth with crack extension, and the crack distribution using measured AE data obtained from the previous V, L, and C1 studies as well as a new C2 UCG model study. Calorific values obtained by the respective models are shown in Fig. 3, from which it is seen that significantly higher calorific values were obtained using linking-hole UCG systems under the given experimental conditions. Further coaxial model experiments were performed under similar conditions for different operational times (14 h for C1 and 19 h for C2) and hole diameters (13 mm for C1 and 30 mm for C2). Data on product gas concentration in the C1 model are not accessible for the period between 5.7 and 7.3 h. For the C2 model experiment, we successfully collected only gas components during the 6.5 h gasification process. As expected, the calorific value of the product gas was higher, and effective combustion lasted longer when a bigger coaxial hole was used.

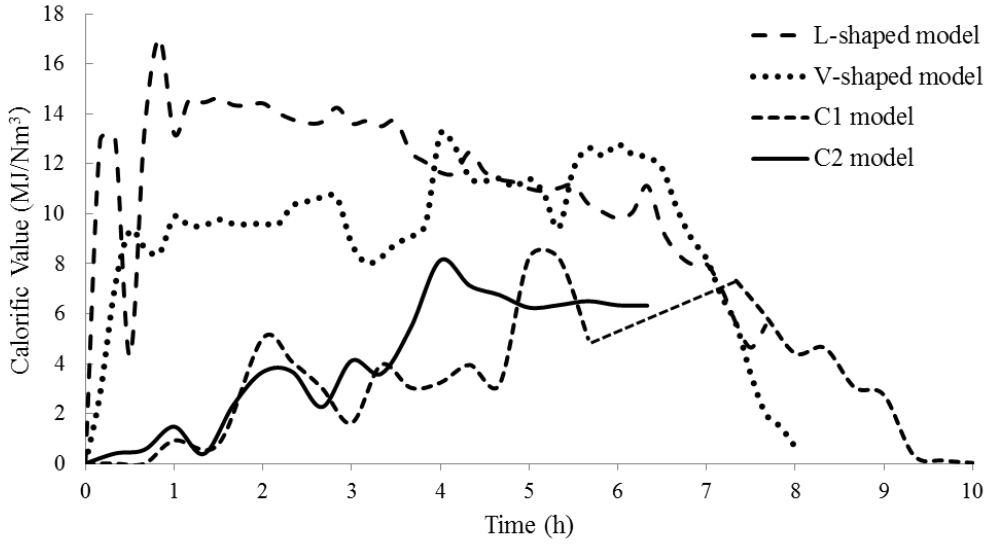

Fig. 3. Calorific values of product gas in L- and V-shaped linking-hole models and C1 and C2 coaxial-hole models.

3.1. Effect of the local temperature on AE count rate and event

Following ignition of the coal, pure oxygen was supplied to enable gasification over the duration of the experiment. In the L-shaped UCG model, two linking holes were formed for gas production: one for injecting gasification agents from the upward side, and the other for exhausting gas production, as shown in Fig. 2. Temperature variation and AE activities that occurred inside the coal block during the experiment are shown in Fig. 4 for the case of the L-shaped UCG model wherein the gasification process was sustained at an oxygen supply rate of 3.8–5 L/min.

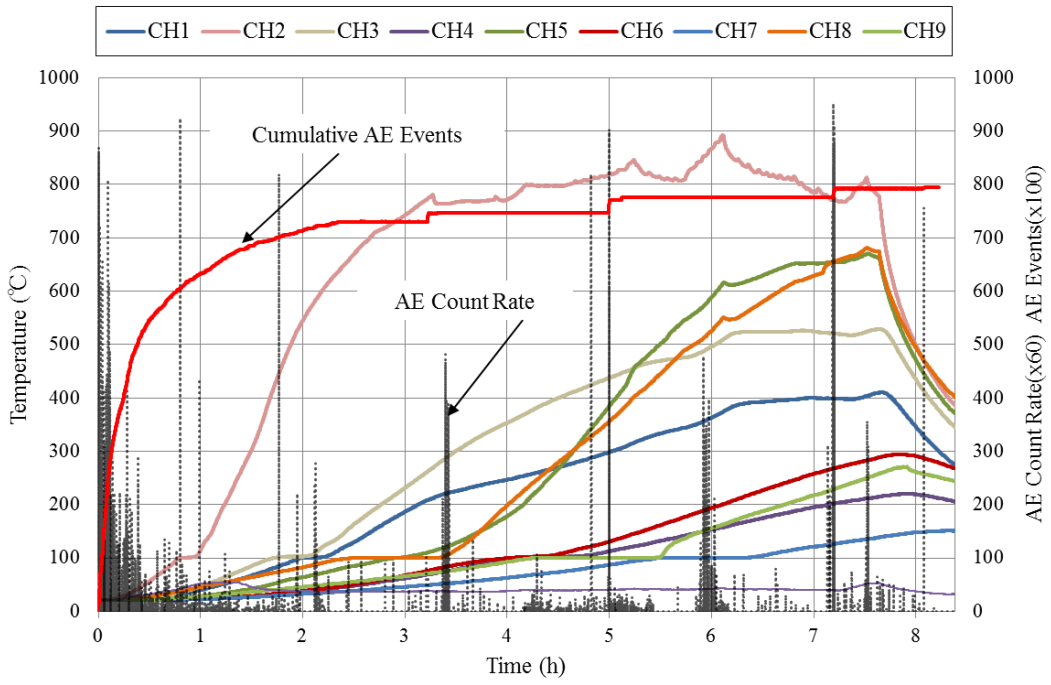

Fig. 4. Variation of AE activities (count rate/event) with temperature change vs. time in L model experiment.

During the experiment, fracturing occurred inside the gasification area under the coal burning. The AE count rate reflects the magnitude of the resulting AE activity, with the number of AE events corresponding to the number of cracks initiated inside the coal samples. During the initial period, the temperature at position CH2 grew rapidly to a high level, which demonstrates that the combustion area was formed near the ignition position. The results demonstrate that the number of AE events and the AE count rate increased rapidly with changing CH2 temperature at the beginning of the experiment. Comparison of several peak values at CH2 with AE events/count rate reveals a mutual correlation, i.e., at the time of local peak temperatures, AE activity was high. During the same time period (0–2 h, Fig. 3), the calorific value of the combustible gas also rose in the L model. Subsequent temperature readings from thermocouples CH1 and CH3 reveal a relatively high growth rate after approximately 2.2 h at each side of the gas inlet. At approximately 3.5 h, the high temperature zone started to move toward the outlet side, as reflected by the rapid increase of the temperature at CH5 and CH8 (Fig. 2). It is also seen that AE activity also occurred and the count rate hit several peaks during these time periods. We stopped the oxygen flow after 7.2 h of operation, resulting in a sudden drop in the temperature of the combustion area with the increment of AE events.

In the V-shaped model experiment, oxygen feed gas was blown into the reactor at a flow rate of approximately 5 L/min in order to heat the coal block and accumulate a sufficient amount of thermal energy for gasification process development. Fig. 5 shows the temperature changes and AE activity occurring within the V model during this test. The results show a cumulative rise in AE events with increasing temperature. The temperature recorded at CH1 maintained relatively higher growth before 3 h of operation, which demonstrated that the combustion area was formed early in the experiment near the ignition area (near CH1) in the early stage. But it can be seen that, after about 2.5 h, the temperature recorded at each thermocouple rose slowly except of the CH1, CH2 and CH7. The higher zone moved along the upper linking-hole (CH2, CH7) in the middle period. This is because an inherent large crack exists in the coal block sample applied in this experiment, which locates in the area between CH2 and CH7 and roughly along the upper linking-hole. Saulov D.N. et al [44] reported the valuable work for investigating the influencing factors of flame behavior (position and propagation) in gasifier, such as primary physical parameters, injection rate, mass balance, etc. by establishing a theoretical model. At about 3.9 h, the flow rate of feeding gas was changed temporarily from 4.5 to 7 L/min. But the gasification zone propagated along the upper linking-hole as before and high temperature zone located around the CH2 and CH7, because the inherent large crack is still the dominant factor at this period. The thermocouple at CH8 was used to measure the temperature of the product gas at the outlet. The CH8 measurements indicate that local temperatures rose gradually, reaching as high as approximately 900 °C; it can be inferred that this highest temperature value is the temperature of the cavity roof, where combustion occurs. The feeding gas flow rate was continuously increased to 8 L/min at about 5h. The temperature around the location of CH3 and CH6 increased abruptly and the gasification zone gradually propagated along the lower liking-hole can be inferred. The AE count rate and number of cracking events increased markedly during the periods of rapid temperature growth between 3.5–4.5 h and 6–7 h; in particular, both measures attained high values at around 4.1, 4.8, and 6.2 h. The recorded temperature of the product gas also changed considerably and peaked around these times. These observations demonstrate that AEs are more significant when the

temperature fluctuates significantly inside the reactor. After rising the flow rate of feeding gas at 4 h; from Fig. 5, it is seen that the temperature increased sharply near this point. Both AE activity and the calorific value of the synthesis gas rose after the oxygen supply rate increase at 4 h (Fig. 3); the results also indicate expansion of the gasification process and combustion area. After more than 8 h of operation, the global temperatures inside the reactor appeared to continuously decline, indicating that the gasification zone arrived at the outlet of the model, likely initiating the termination of the gasification process.

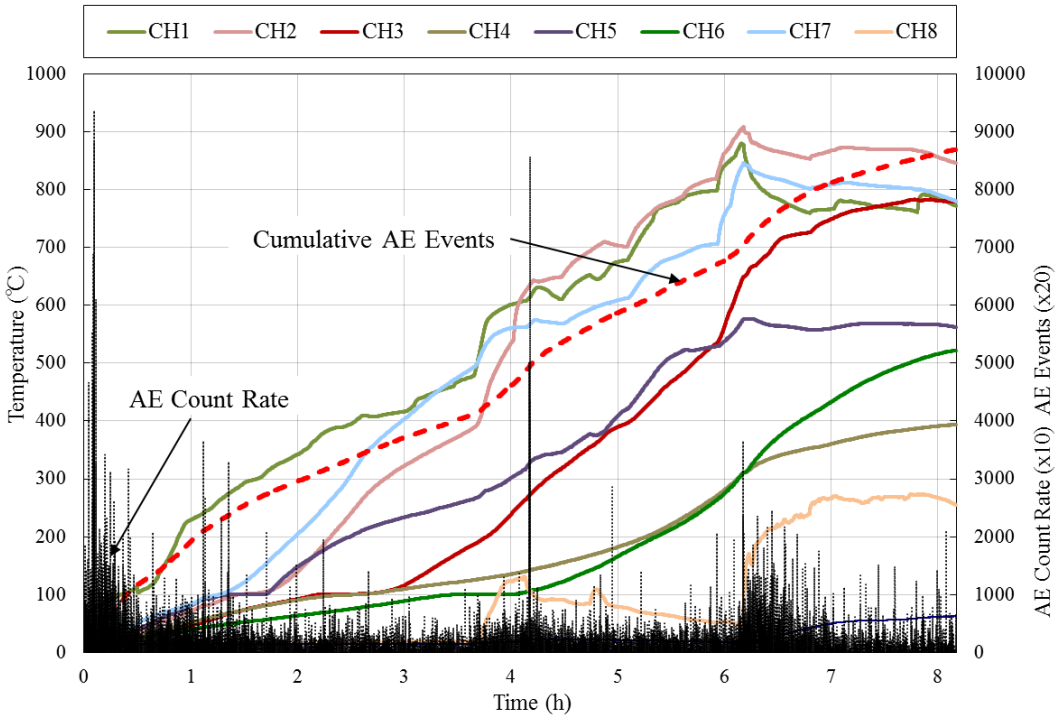

Fig. 5. Variation of AE activities (count rate/event) with temperature change vs. time in V model experiment.

For comparison, coaxial-hole model experiments were conducted in the laboratory using similar operating parameters to those used in the oxygen-fired V- and L-shaped model experiments just described. In a general UCG system, two boreholes, for air/oxygen injection and gas production, are drilled from the surface to the target coal seam using a linking hole as gasification channel. However, under complex coal seam conditions, traditional linking methods may be unusable or uneconomic. The coaxial-hole UCG method is expected to be useful for producing local energy in small communities because of its wide tolerance to environmental geological conditions and because the costs of constructing a single coaxial drill hole and ground plant facility are lower than those of conventional UCG using a linking hole.

Fig. 6(a) shows the temperature increase at CH2–CH8 measured throughout the combustion process and the AE activity as a function of operation time for a C1 coaxial-hole model experiment. The temperature profiles of CH1 and CH9, which detected the temperatures of the gasification channel and the gas stream, are shown in Fig. 6(b).

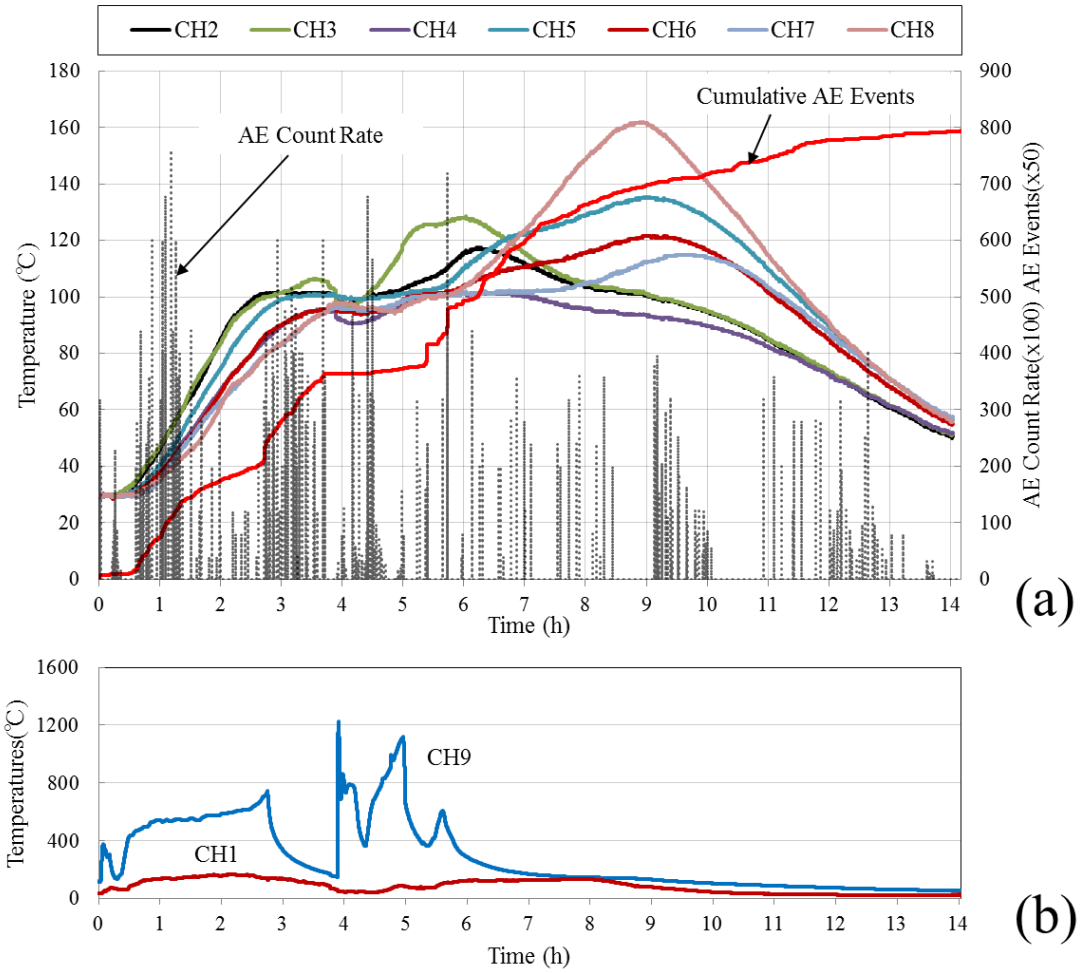

Fig. 6. Variation of AE activities (count rate/event) with (a) temperature change vs. time and (b) temperature profiles in gasification channel/product gas outlet vs. time in C1 model experiment.

Gasification carried on for approximately 14 h at the operating parameters used in the experiments described above, with a changing flow rate averaging 4.0 L/min. The results show that the number of AE events and the AE count rate increased rapidly in the early stage of the experiment as the temperature rose inside the model. It is apparent that the AE events and AE count rate were active during the initial part of the experiment. The temperature at CH3 steadily increased to approximately 100 °C, indicating the temperature of the corresponding coal block surface; from this, the formation of a combustion area near the ignition area (i.e., near CH3) can be inferred. After approximately 3.25 h, the experiment was stopped for approximately 30 min, which caused the temperature of the reactor to drop and resulted in a considerable increase in AE events. After about 5 h and 7 h, the temperatures recorded by thermocouples CH2 and CH3 and by thermocouples CH5 and CH6 gradually increased and reached respectively high levels. It can be seen that the gasification zone gradually propagated from bottom to the upper part. Two peak calorific value values (Fig. 3) were obtained during these two time periods. After this, the temperature at CH8 continued to rapidly grow to its highest value, corresponding to a relatively high AE count rate, which depicts the reaction zone has arrived at the top of the model. During the course of this later period, a gradual drop in temperatures in the gasification zone was observed, indicating that the reaction area had moved to the coal block border.

The C2 model experiment was conducted using a mixture of air and oxygen (with an oxygen concentration of approximately 35%) as a gasification agent. At 0–6 h, the air/oxygen was injected into the gasifier at an average flow rate of approximately 10.0 L/min. During the remainder of the process, only air was provided for gasification. Variations of temperature and AE occurring in the C2 model are shown in Fig. 7(a). The temperature profiles of CH1, CH2, and CH3 (Fig. 7(b)) show the growth of the gasification channel (as shown in Fig. 2) from the bottom to the top part of the coaxial hole. After beginning, thermocouples of CH5 recorded a relatively high temperature, it can be inferred that the combustion area was formed around the bottom of model (ignition position). Three hours after the start of high AE activity in the initial phase, the temperatures of the thermocouples rose considerably. After about 4 h, and again after 6 h, the temperatures of CH 4–6 and CH 7–8 respectively increased rapidly and reached the highest value. It shows that the combustion zone moved from the lower part to the top part of the coal block. This result also can be clearly seen in Fig. 7(b), the temperature recorded by CH1, CH2 and CH3, had a significantly increase respectively at about 1.6 h, 4 h and 6 h. The oxygen supply was terminated at approximately 6.5 h, causing a large drop in local temperatures inside the reactor and a high amount of AE. After 10 h, the temperature of the gasification area stabilized at a lower level, which was only possible because the reaction gas had been switched from air/oxygen to air. By this point, the AE count rates had also diminished significantly. Nevertheless, effective coal combustion and stable gasification were attained during the process.

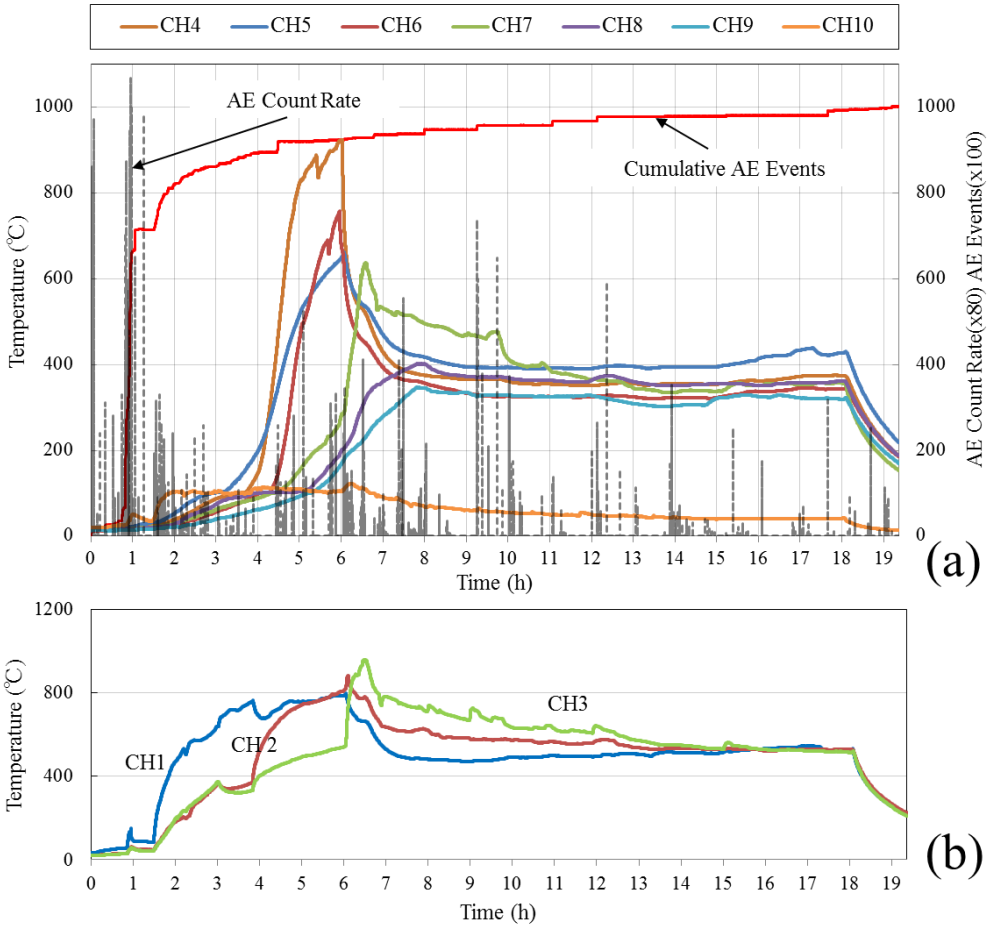

Fig. 7. Variation of AE activities (count rate/event) with (a) temperature change vs. time and and (b) temperature profiles in gasification channel vs. time in C2 model experiment.

The experimentally obtained results demonstrate that many AE events were generated during coal combustion and that the AE activity was closely related to changes in local temperature inside the coal. The AE events seem to have resulted from crack initiation and extension around the coal combustion area under the influence of thermal stress. The number of AE events generated with increasing temperature within the laboratory UCG models was analyzed using statistical methods, as shown in Fig. 8. To determine the relation between AE activity and local temperature change, the countable number of AE events occurring within temperature intervals incremented by 50 or 100 °C were investigated using the AE results obtained from the UCG experiments conducted in this and in our previous study. Variation of AE events during the successive temperature phases was recorded, with data collected during the coal ignition process excluded because the crack numbers during this phase could have been affected by the ignition method and intensity. In Fig. 8, the dots show averages of AE events, and the vertical bars show standard deviations. An examination of the figure reveals that the relation between AE events and temperature under the experimental operating conditions can be roughly described as a polynomial approximation curve. This result indicates that the fracturing activity is proportional to the temperature increment, a relation that can be regarded as resulting from the coal-fracturing mechanism occurring during combustion. Although the time dependence is not described in this figure, the increase in amount of the microcracks will progressively slower and eventually trend to be stable after a long time of operation and without a fast movement of combustion zone. This is also investigated adequately in our past works [54] by evaluating the AE occurring of coal samples under various heating process. The occurred crack volume and density also affect the further development of microcracks with AE. It was found that the cumulative events show a cavity growth deceleration when a certain amount of cracks are generated inside the coal; this is also the reason why high AE count rates were observed in the initial period, while fewer and relatively weak cracks were detected during the burning stabilization stage.

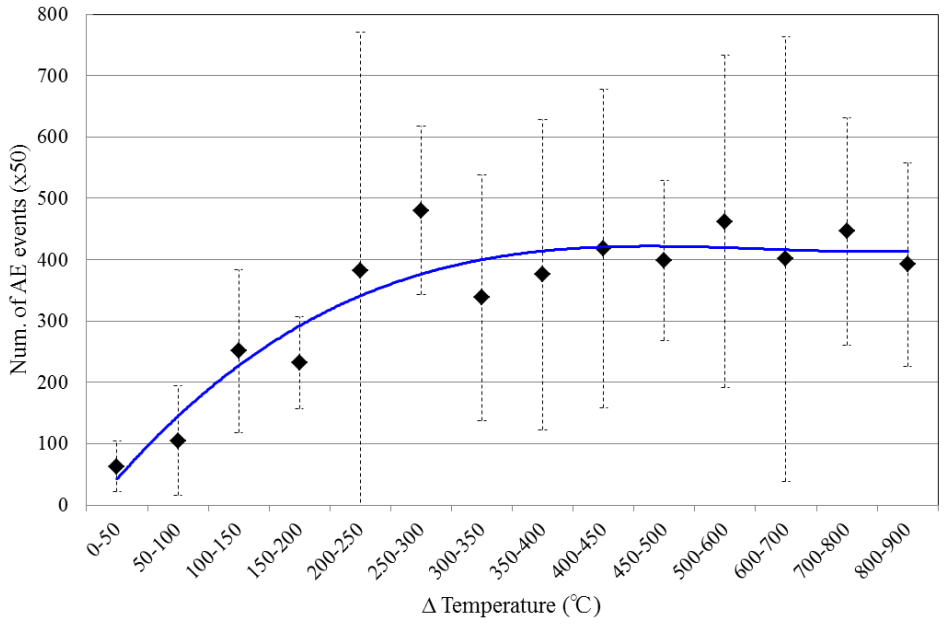

Fig. 8. Variation of AE event generation at different temperature intervals under experimental conditions.

3.2. AE source location and crack distribution model

As described above, real-time monitoring of AE events and the variation of the AE count rate during the gasification process can identify the extent of fracturing inside the reactor and can even provide an early warning for excessive fracturing in the coal. It was established that the local temperature change strongly affects AE activities caused by fracturing. The cumulative number of AE events changes linearly as the AE count rate increases, and fractures apparently correspond to the number of events that are generated inside the reactor. Furthermore, the cumulative events curve shows a similar form to the coal-temperature curve. To better correlate this AE data with individual cracks within the coal, we further analyzed the results in terms of AE source location and moment tensors.

3.2.1 AE source location

The AE source location can be determined from the differences between the arrival times of waves measured at each AE sensor. Fig. 9 shows a flow chart of the localization algorithm. The program is fed the relative coordinates of sensors in each UCG model. For the initial configuration, it is necessary to calculate the primary wave velocity using a striking test (artificial seismic source) prior to the experiments because the density of the simulated coal seam inside the UCG model is inhomogeneous. As the ray path can be assumed to be linear, a constant primary wave velocity was employed within the localization algorithm.

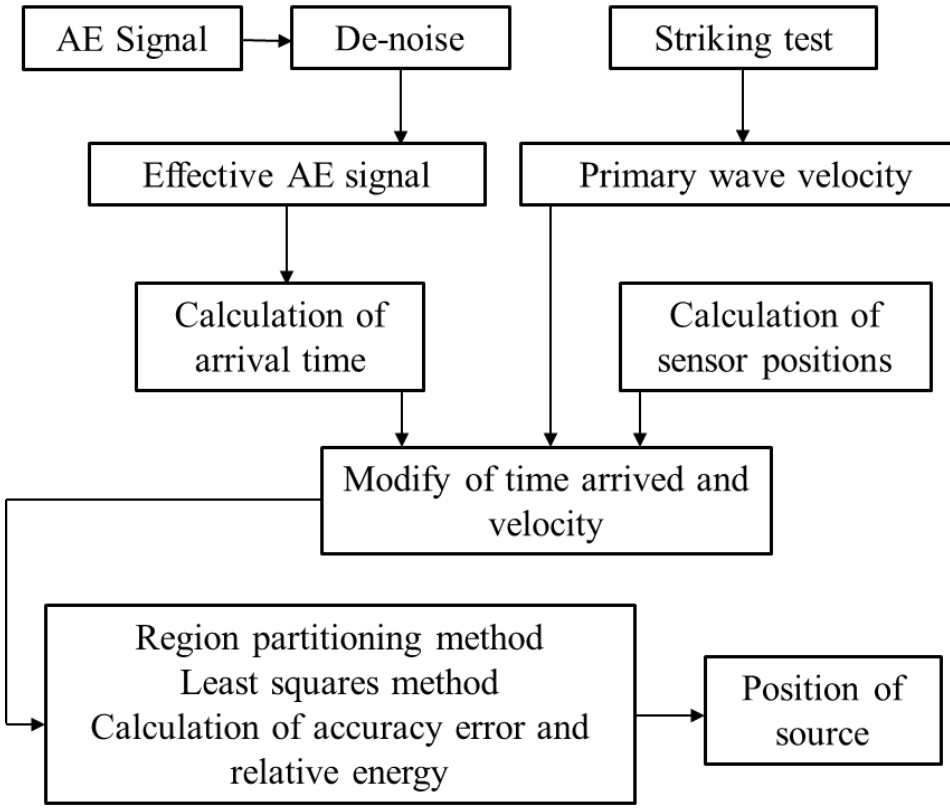

Fig. 9. Flow chart for AE source location algorithm.

We can determinate the P-wave arrival time at each sensor from the recorded AE waveforms, as shown in Fig. 10. The arrows on each sensor's waveform indicate the onset time of the P-wave, i.e., the crack initial motion. The relative energy emitted from each crack can be estimated from the square of the maximum amplitude of the waves. Prior to AE source location, AE signals are filtered in order to remove noise signals generated by adjustment operations during the experiment. The least-squares iteration algorithm [55–57] is then used to calculate the position of the AE source according to the respective sensor coordinates and the primary wave arrival times.

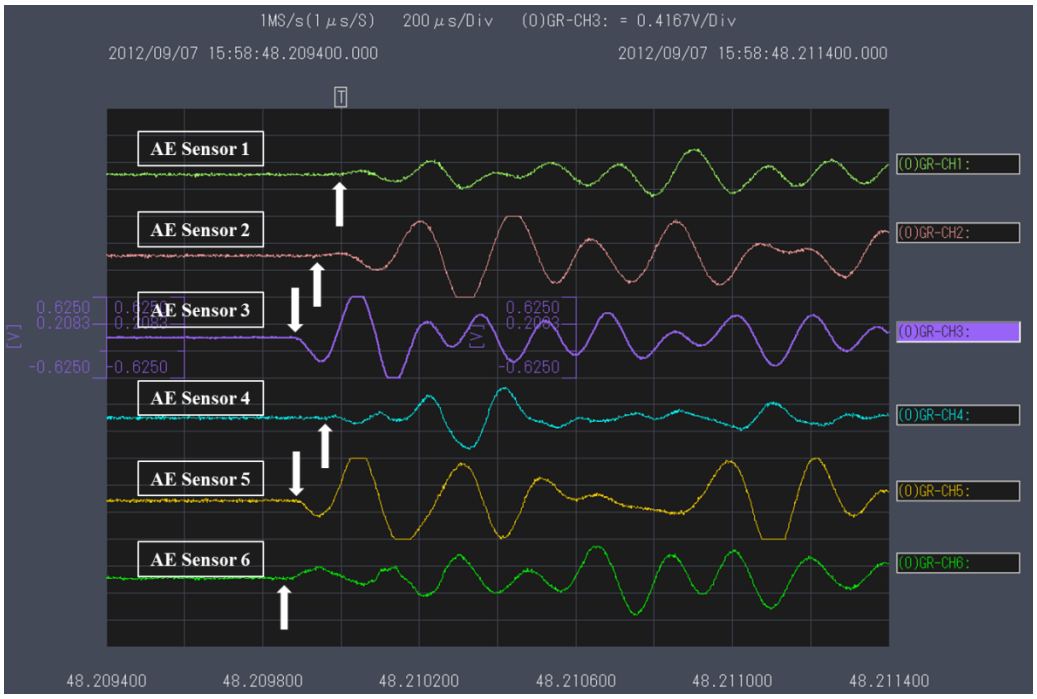

Fig. 10. Determination of P-wave arrival time (typical signals for an AE source).

AE sources located in the above-described UCG model experiments are shown in Fig. 11. The red, green, and blue spheres in the figure depict the AE sources in the early, middle, and later periods, respectively. The extent of damage, i.e.,., the relative energy emitted from cracking, can be differentiated based on sphere sizes, and the extent and movement of combustion and the gasification scope inside he coal blocks can be deduced from the AE source locations. In the early stages of the experiments, the AE sources are mainly concentrated around the ignition points. Subsequently, the AE source clouds spread and move along the linking holes during the middle periods. Intense AE clouds are observed in later stages, with fractures spreading and diffusing perpendicular to the direction of the gasification channel. It is apparent that the gasification zone in the L model test expanded from the gas inlet to the central region and became enlarged around the gasification channel. At the early stage of the V model experiment, the AE sources clustered around the left linking hole, suggesting that the fracturing process inside the gasification area and the AE clustering region was strongly governed by the inherent inhomogeneity of the coal block. The AE source results from the coaxial models indicate that the gasification areas evolved from the bottom to the top part along the coaxial hole. In particular, the C2 model experiment achieved more efficient combustion, with a larger gasification channel and a longer operational time, than did the C1 model.

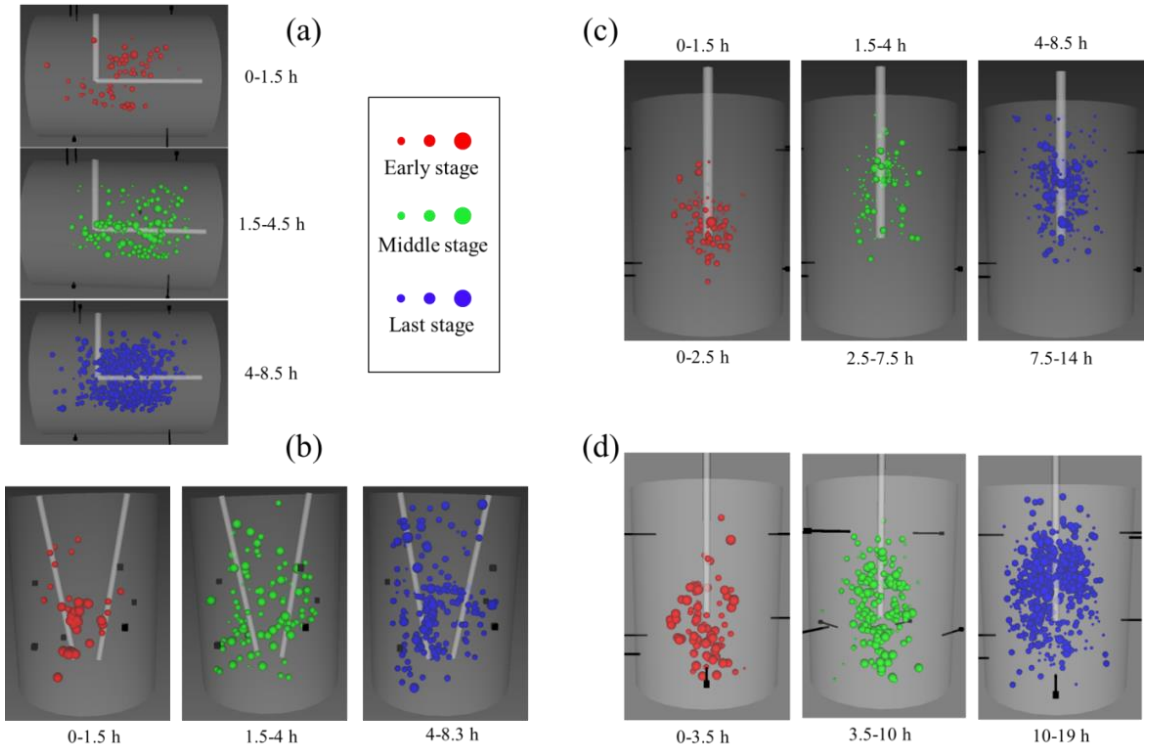

Fig. 11. Results of AE source location in ex-situ reactors for (a) L model, (b) V model, (c) C1 model, and (d) C2 model.

The movements of the centers of gravity within the AE cloud were then investigated (Fig. 12) based on the results of AE source locations. ~~The velocities of cavity growth along the linking hole estimated by the AE cloud movement in the respective models are provided in Table 1.~~ The colored circular rings in the figures represent the centers of gravity of the AE cloud calculated using the statistical approach based on the product of the relative AE source energy and the event count. The lengths of the arrows in the horizontal and vertical directions represent the breadth of the AE cloud region.

The AE cloud movement was reconfirmed by the center of gravity coordinates of the AE sources; in each time period, the AE cloud movement seems to reflect that of the combustion and gasification region and the cavity growth within the coal. We investigated the distribution of AE sources within three different regions (0–40 mm, 40–80 mm, and 80 mm from the reactor boundary). The flame propagations in these models are also described with the mobility centers of the high temperature zone, as show in this figure. This was roughly estimated using the peak values and combined with the high temperature distribution of local thermocouples at the specific time points. It can be seen that although some level of positions difference exists, the high temperature zone moved broadly consistent with the center of gravity of AE cloud. For a more precise estimation of central position of high temperature zone with temperature data, the higher density arrangement of thermocouples in the model is required. Even so, the movement of AE cloud centers is also proved supporting the observation results

The velocities of cavity growth along the linking hole estimated by the AE cloud movement and local temperatures in the respective models are provided in Table 1. The comparison results show that the similar propagation speeds were obtained in these models except the L model. In the L model, the moving range of the AE cloud in horizontal direction (perpendicular to the linking-hole) has no obvious change compared to the propagation along the linking-hole, which caused a relatively lower

value of velocity calculation. Despite this, the AE cloud in this model can reflect the region and movement of the gasification zone accurately yet.

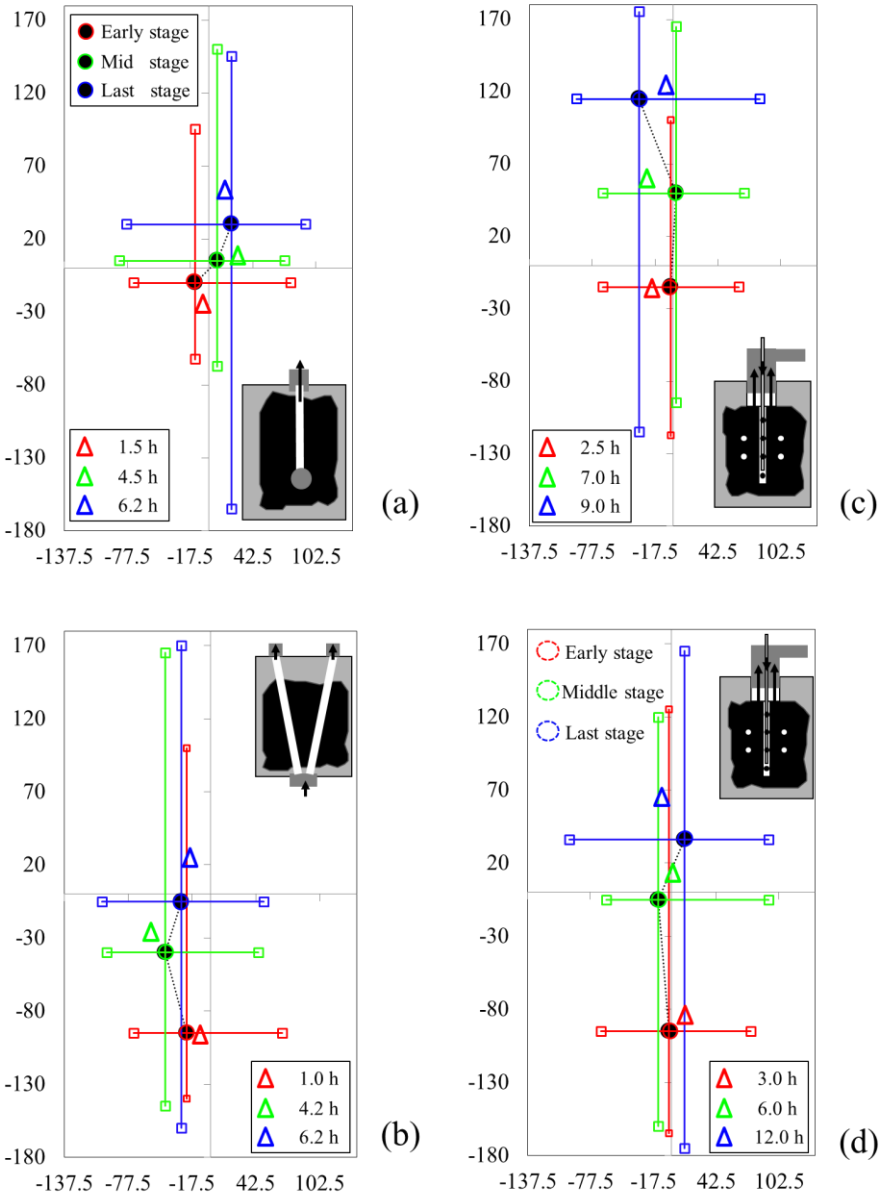

Fig. 12. Results of AE cloud center evolution in ex-situ reactors for (a) L model, (b) V model, (c) C1 model, and (d) C2 model. (Colored circular rings denote the centers of gravity of AE cloud; Colored triangles denote the estimated high temperature zone centers.)

Table. 1. Estimation of cavity growth velocities in the ex-situ reactors for (a) L model, (b) V model, (c) C1 model, and (d) C2 model.

Model No.	L-shaped (L)	V-shaped (V)	Coaxial (C1)	Coaxial (C2)
Velocity of Cavity Growth (cm/h) with AE cloud center	0.8	2.1	1.9	3.9
Velocity of Cavity Growth (cm/h) with local temperature	2.0	2.5	1.8	3.1

The relative energy of sources obtained from the AE parameters was regarded as a damage index, as shown in Fig. 13. It is seen that AE sources with high energy clustered around the linking hole (0–40 mm) in the L and V models. The maximum clustering of relatively intensive AE was concentrated in the region between 40–80 mm, except for the C1 model (Fig. 13(c)). This was because fracturing and coal spalling were generated in the vicinity of the cavity roof and developed along with the damage progress. In the C1 model, a significant number of sources with lower relative energy (<0.001) clustered in regions close to the coaxial hole. AE activity in terms of energy and quantities was higher in the C2 model than in the C1 model under the same experimental conditions.

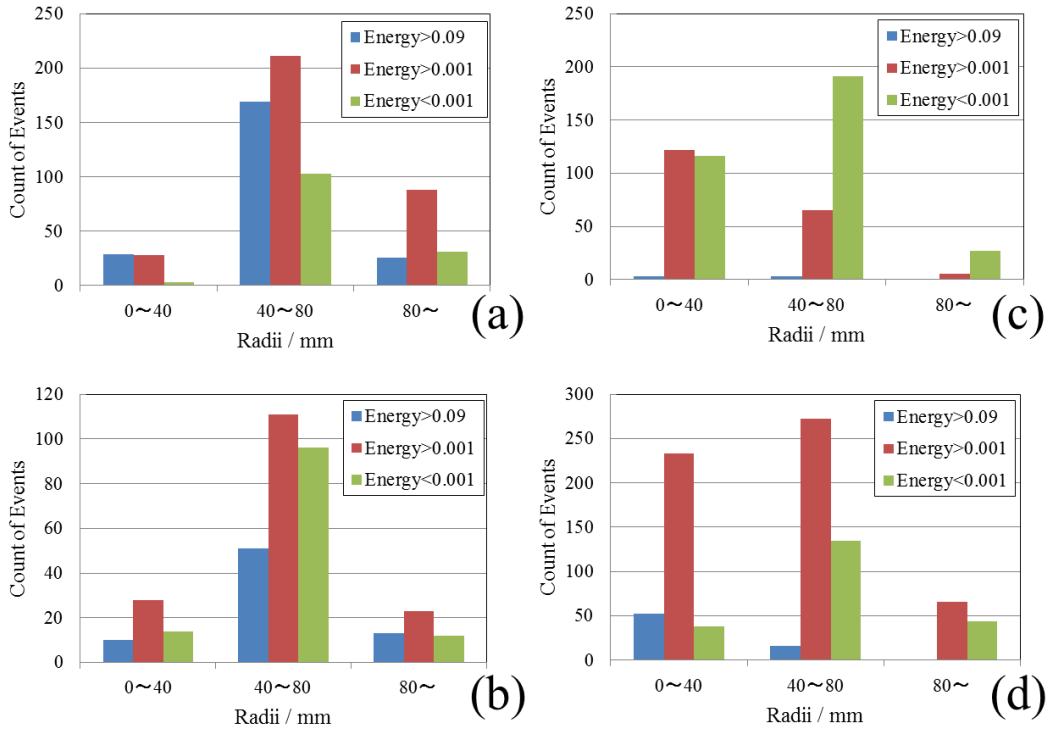

Fig. 13. Estimation of AE source (relative energy) distributions at different regions around gasification channel in ex-situ reactors for (a) L model, (b) V model, (c) C1 model, and (d) C2 model.

As discussed above, the locations of the AE sources visually correlated with crack initiation and extension inside the coal. The AE cloud center movement also reflected the combustion area size and the cavity growth in the gasifier. The AE sources and crack distribution models show that most cracks were generated at the fracture position and around the combustion area. The region where the AE sources clustered also corresponded to the local high-temperature zones measured by thermocouples.

3.2.2. Moment tensor analysis

As discussed above, AE parameter analysis was used to evaluate crack initiation and extension under UCG operation based on monitored waveforms and parameters such as count rate, event occurrence, relative energy, etc. We then quantitatively estimated cracking and damage mechanisms in coal during the gasification process using moment tensor analysis [58, 59] of the AE results of located AE sources. Arrival times and amplitudes of crack initial motions were determined and 3D source location models were obtained using differences in arrival times at each sensor. Based on the

amplitudes, moment tensor components were then calculated, and the source time function was calculated using the moment tensor components [60, 61] under the assumption of the Haskell slant function [62]. Using this information, crack distribution models were constructed from the obtained source time function based on the Combined Geometric-Mechanical Models (proposed by Ivanova) [63]. This procedure allowed us to determine the proportion of shear and tensile crack contributions on the AE sources and to classify cracks by types of dominant motion. By modeling cracks as disks with zero thickness, moment tensor analysis allowed us to obtain information on source type and orientation. Such analysis can provide quantitative information on the 3D location of cracks, crack type, crack orientation, and the direction of crack motion, and makes it possible to visualize the cracking process inside the UCG gasifier.

Crack distribution models estimated using the moment tensor analysis are shown in Fig. 14. The cracks are represented by multipronged disks in the 3D crack distribution models. Tensile- and shear-type fractures can also be confirmed. Pink and blue disks represent, respectively, tensile and shear fractures, with mixed-mode fractures indicated by gradients of purple and yellow. The center of each crack disk is located at the coordinates of its respective AE source location, and the disk radii show the relative AE energy. Corresponding to the AE source location results, the L-shaped linking-hole model cracks were generated in the early stages mainly around the ignition area, after which the cracking area extended to the central part. In the L and V models, cracks were spread widely all over the reactor as the damage progressed in the gasification process. In the C1 model, cracks were mainly concentrated in a limited region around the coaxial hole in the middle-upper part of reactor. In the C2 model, cracks were located over a wider area and many AEs occurred all over the reactor, from the bottom to the top part, along the coaxial hole.

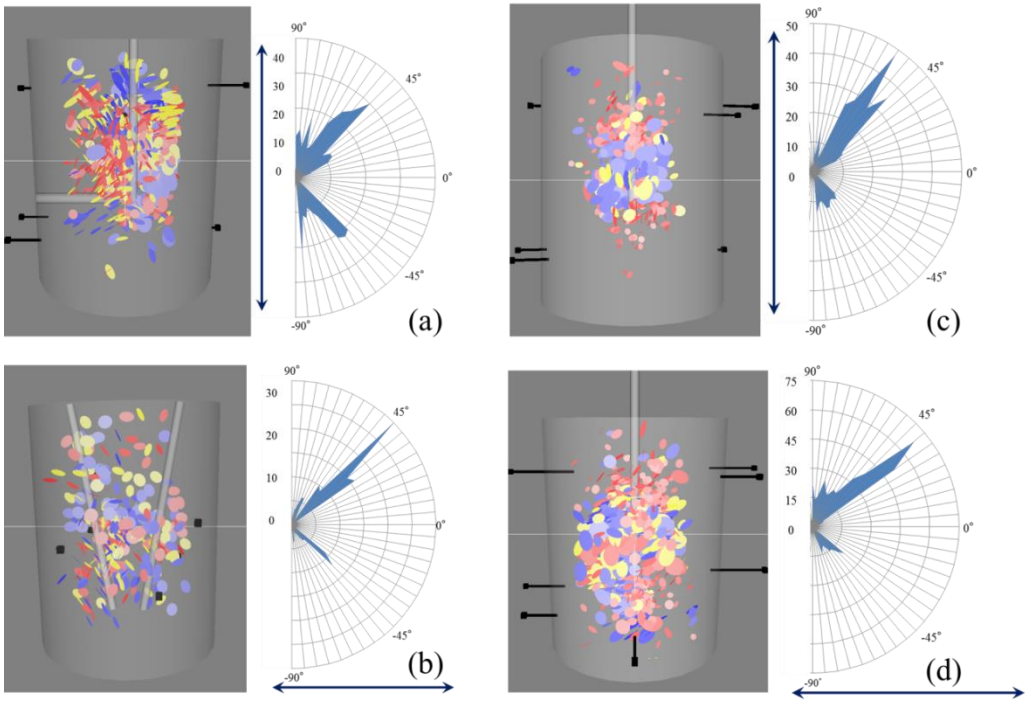

Fig. 14. Results of moment tensor analysis and directions of tensile crack motions in ex-situ reactors for (a) L model, (b) V model, (c) C1 model, and (d) C2 model (arrow shows direction of stratified plane of coal).

The crack distribution models revealed what type of crack was dominant inside the coal block. Table 2 lists the number of tensile, shear, and mixed-mode cracks identified by moment tensor analyses of the four experiments. To estimate the fracture mechanism from the cumulative damage induced by the gasification process, we also assessed the ratio of each type of crack. In the early and middle stages of the L model, tensile-type cracks are highly represented (55.4%/53.9% > 23.0%/35.5%) around the linking hole. The ratio of shear cracks in the V model slightly increases from the middle (33.7%) to the later stage (39.7%). By contrast, the ratio of tensile cracks decreases from the middle (49.0%) to the later stage (32.5%). It was determined that the cracking behavior produced over the three stages by the C2 model represented by the contribution of tensile and shear mode cracks was more significant than in the C1 model owing to differences in operational conditions (radius of drilling hole, feed gas rate, and operation time) applied in the respective experiments. Our results also show that tensile failure occurred through a major microscopic failure mechanism in the vicinity of the gasification channel.

Table. 2. Compositions of each crack type (tensile-, shear-, and mixed-type cracks) in ex-situ reactors.

	Early stage			Middle stage			Later stage		
Model No.	Tensile-type crack (count)	Shear-type crack (count)	Mixed-type crack (count)	Tensile-type crack (count)	Shear-type crack (count)	Mixed-type crack (count)	Tensile-type crack (count)	Shear-type crack (count)	Mixed-type crack (count)
L (L-shaped)	41 (55.4%)	17 (23.0%)	16 (21.6%)	76 (53.9%)	50 (35.5%)	15 (10.6%)	233 (40.7%)	209 (36.6%)	130 (22.7%)
V (V-shaped)	30 (51.7%)	16 (27.6%)	12 (20.7%)	51 (49.0%)	35 (33.7%)	18 (17.3%)	39 (32.5%)	83 (39.7%)	47 (27.8%)
C1 (Coaxial)	97 (52.7%)	56 (30.4%)	31 (16.9%)	126 (70.8%)	35 (19.7%)	17 (9.6%)	92 (50.6%)	65 (35.7%)	25 (13.7%)
C2 (Coaxial)	26 (46.4%)	17 (30.4%)	13 (23.2%)	54 (43.6%)	46 (37.1%)	24 (19.3%)	283 (47.9%)	187 (31.6%)	121 (20.5%)

As shown in Fig. 14, the directions of the crack faces were also investigated. The arrows on the right-hand figures show the general direction of the stratified plane of coal. The linking holes in the L and C1 models were drilled parallel and as closely as possible to the stratified plane of the coal block. By contrast, the drilling holes were set as nearly perpendicular to the stratified plane as possible in the V and C2 models. In the L and C1 model experiments, the dominant crack motion directions (tensile cracks only) concentrated primarily at between 50° and 90° to the stratified planes (Fig. 14(a) and 14(c)). Similarly, the major directions of crack motion in the V and C2 models coincided with the major stratified planes (25°–45°) (Fig. 14(b) and 14(d)). As a result, the dominant failure directions in these gasification processes were close to the direction of the major stratified plane of coal. Fig. 15

shows the distribution of dominant failure in different regions. The figure indicates that shear-type cracks clustered around the linking hole (0–40 mm) in the central region, while tensile-type cracks were distributed outward from the combustion region (40–80 mm and 80 mm). The shear- and tensile-mode cracks comprised 75%–85% of the total sources. These results indicate that the different temperature fields of distinct locations within the reactor induced differential fracturing behavior in the coal. The percentages of tensile/shear cracks are almost identical among the UCG models, which shows that the ratios of the two crack types did not differ significantly in the coal under the gasification process.

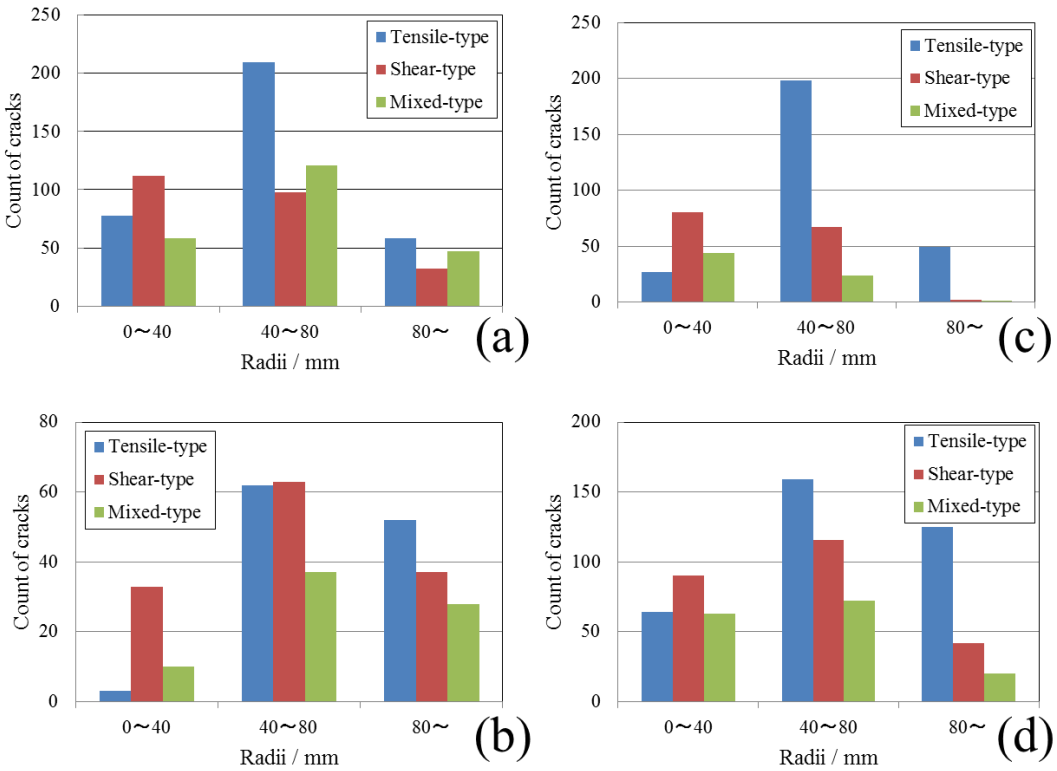

Fig. 15. Estimation of crack (tensile-type crack, shear-type crack and mix-mode crack) distributions at different regions around gasification channel in ex-situ reactors for (a) L model, (b) V model, (c) C1 model, and (d) C2 model.

3.2.3. Implement of AE in real UCG

For optimizing the UCG operations and reducing the potential risks of environment and underground water, it is necessary to monitor the gasification process and understand the fracturing activities occurring in the coal seam, particularly in the zone near the gasification cavity exposed by the propagation of the combustion fracture. In our study, acoustic emission (AE) technology was employed as a supplement to traditional measurements, e.g., temperature and gas, in order to monitor fracturing and cavity evolution during the UCG process.

For the in situ UCG, a real-time monitoring and control system is necessary for safe and efficient gasification. From our study, the AE technology is verified as a reliable approach for monitoring and evaluating the gasification process in laboratory-scale UCG when combined with the traditional measurements. For the real UCG, a type of transducer with the low frequency micro-seismicity, i.e., a

geophone, which is functionally similar to the AE accelerometer employed in this study, could be used for monitoring the fracturing activity and gasifier's structure in underground. The geophone is a ground motion transducer that can convert the ground damage and movement in the voltage signal. Any deviation in this measured voltage from the base line is regarded as micro-seismic response, which is used for analyzing the structure of underground gasifier in coal seam. As with the AE sensor, parameters such as event, count rate, and relative energy can be obtained from the geophone by processing the recorded voltage signals. Many different types of geophone are now being manufactured nowadays and are used for the measurement of machine vibration, earthquakes, oil exploration, and conventional mining. In our follow-up study of UCG, the new-type three-component geophones will be employed, which is called borehole geophone. This moving coil type geophone is constituted by two components horizontal and one component vertical and potentially provides the higher precision 3-D fracture exploration during real gasification process in underground coal seam.

4. Conclusions

The ex-situ experiments were conducted in order to simulate UCG under several distinct linking-hole UCG models. AE was used to monitor crack initiation and extension and cavity evolution inside the combustion reactor during the gasification process. Our conclusions are as follows:

1) This study investigated the effects of various linking-hole types and radii, operation times, feed gases, and flow rates on gasification. We confirmed that these operational conditions significantly affect facture occurrence, crack behavior, cavity growth inside the gasifier, and gasification efficiency.
2) AE parameter analyses of, e.g., count rate and event occurrence, show that there is a large difference in AE activities under different temperatures during the damage process and between distinct models. The active periods of AE occurrence coincided with local temperature changes over time. These results reveal that AE activity is closely related to the temperature change occurring inside the coal, with AEs apparently resulting from the crack initiation and extension influence of thermal stress.
3) AE source locations, as determined in this study, could be used to characterize fracture occurrence and crack extension in UCG models in a direct manner. The mobility of the AE cloud center can be derived from the count and relative energy of sources using a statistical approach; by doing this, it is possible to represent high-temperature-zone movement and to estimate the velocity of gasification cavity growth.
4) The crack distribution model constructed via moment tensor analysis was shown to be effective in understanding the fracturing mechanism of the UCG process. This model can provide quantitative information on the three-dimensional location of cracks, crack types, and orientations of crack initiation in coal during the UCG process.
5) The moment tensor analysis revealed that tensile failure was a major fracture mechanism of coal that became more dominant as the damage progressed during the gasification progress. The distribution of failure modes (tensile/shear cracks) in different regions of the reactor showed that the shear failure was concentrated in the vicinity of the gasification channel.

6) In addition, the general direction of the failure face of the cracks clustered in the reactor could be estimated from crack distribution. We found that the dominant failure directions in these models were close to the direction of the major stratified plane of coal.

The application of the AE technology during UCG is effective for monitoring the gasification process and can play a very important role as a quantitative method for analyzing cracking behaviors and understanding the fracture mechanism in the coal gasifier. AE monitoring makes it possible to visualize cracking processes and cavity evolution inside UCG target coal seams.

Acknowledgements

This study was supported by the Japanese Society on UCG, Mikasa City, Center of Environmental Science and Disaster Mitigation for Advanced Research of Muroran Institute of Technology and the Grant-in-Aid for Scientific Research (b), 21360441 from the Ministry of Education, Culture, Sports, Science and Technology (MEXT), Japan. The authors gratefully acknowledge their support.

References

[1] IEA, “Energy Balances of OECD Countries 2013”, 2013.
[2] IEA, “Energy Balances of Non-OECD countries 2013”, 2013.
[3] Endo H, Koyanagi N, Harada M. Present situation and issues of coal and coal preparation in India. Journal of MMIJ 2008;124(12):885–9.
[4] Coal in the Energy Supply of India. International Energy Agency. 2002, International Energy Agency, Industry Advisory Board.
[5] Burton E, Friedmann J, Upadhye R. Best practices in underground coal gasification. Lawrence Livermore National Laboratory: Livermore, CA, USA, 2006.
[6] Shafirovich E, Varma A. Underground coal gasification: A brief review of current status. Ind Eng Res 2009;48:7865–75.
[7] Alexander YK. Early ideas in underground coal gasification and their evolution. Energies 2009;2(2):456–76.
[8] Khadse A, Qayyumi P, Mahajani S, Aghalayam P. Underground coal gasification: A new clean coal utilization technique for India. Energy 2007;32:2061–71.
[9] Kapusta K, Stan Czyk K. Development conditions and limitations of the underground coal gasification in Poland. Chem Rev 2009;88:331–8.
[10] Olateju B, Kumar A. Techno-economic assessment of hydrogen production from underground coal gasification (UCG) in Western Canada with carbon capture and sequestration (CCS) for upgrading bitumen from oil sands. Appl Energy 2013;111:428–40.
[11] Yang L, Liang J, Yu L. Clean coal technology – study on the pilot project experiment of underground coal gasification. Energy 2003;28:1445–60.
[12] Prabu V, Jayanti S. Underground coal-air gasification based solid oxide fuel cell system. Int J Appl Energy 2012;94:406–14.
[13] Shafirovich E, Varma A. Underground coal gasification: a brief review of current status. Ind Eng Chem Res 2009;48:7865–75.

[14] Upadhye R, Burton E, Friedmann J. Science and technology gaps in underground coal gasification. Lawrence Livermore Laboratory, University of California, Livermore, California 222523, 2006.
[15] Friedmann, S. J. North America Prospects for UCG in a Carbon Constrained, Energy Secure World. Presented at the Twenty-Fifth Annual International Pittsburgh Coal Conference, Pittsburgh, PA, Sep 29-Oct 2, 2008; Paper 26-1.
[16] Blinderman, M. S.; Friedmann, S. J. Underground Coal Gasification and Carbon Capture and Storage: Technologies and Synergies for LowCost, Low-Carbon Syngas and Secure Storage; Report UCRL-ABS-218560; Lawrence Livermore National Laboratory: Livermore, CA, 2006.
[17] Li H, Yan J, Yan J, Anheden M. Impurity impacts on the purification process in oxy-fuel combustion based CO2 capture and storage system. Appl Energy 2009;86:202–13.
[18] Hu Y, Yan J. Characterization of flue gas in oxy-coal combustion processes for CO2 capture. Appl Energy 2012;90:113–21.
[19] Collot AG. Prospects for hydrogen from coal. IEA Coal Research. The Clean Coal Centre, London, U.K., 2003
[20] Stanczyk K, Kapusta K, Wiatowski M, Swiadrowski J, Smolinski A, Rogut J, et al. Experimental simulation of hard coal underground gasification for hydrogen production. Fuel 2012;91:40–50.
[21] Stanczyk K, Smolinski A, Kapusta K, Wiatowski M, Swiadrowski J, Kotyrba A, et al. Dynamic experimental simulation of hydrogen oriented underground gasification of lignite. Fuel 2010;89:3307–14.
[22] Verma A, Kumar Amit. Life cycle assessment of hydrogen production from underground coal gasification. Appl Energy 2015;147:556–68.
[23] Friedmann SJ. Carbon sequestration. In: Proc. 2006 Energy Symposium, Madison, WI, USA, 2006.
[24] Siemens CW. On the regenerative gas furnace as applied to the manufacture of cast steel. J Chem Soc 1868;21:279–310.
[25] Mendeleev DI. Collected Works XI. Akademiya Nauk SSSR: Moscow, USSR, 1949.
[26] Mendeleev DI. Collected works XII. Akademiya Nauk SSSR: Moscow, USSR, 1949.
[27] Betts, A.G. Method of utilizing buried coal, U.S. Patent 947,608, filed 1906, issued 1910.
[28] Betts, A.G. Process of gasifying unmined coal, Canadian Patent 123,068, filed 1909, issued 1910.
[29] Betts, A.G. An Improved Process for Utilizing Unmined Coal. UK Patent 21674, filed 1909, issued 1910.
[30] Jolley LJ, Booth N. The underground gasification of coal. Survey of the literature. Fuel 1945;24:31–7, 73–9.
[31] Olness DU, Gregg DW. Historical development of underground coal gasification. Technical Report UCRL-52283, California University, Lawrence Livermore Lab: Livermore, CA, USA, 1977.
[32] Ignatieff A. Underground gasification of coal: Review of progress. Trans Can Inst Mining Met Mining Soc Nova Scotia 1949;LII:265–71.
[33] Perkins G, Sahajwalla V. Steady-state model for estimating gas production from underground coal gasification. Energy Fuels 2008;22:3902–14.
[34] Liang J, Liu S, Yu L. Method of stably controlling the process of underground coal gasification [J]. Joural of China University of Mining & Technology. 2002;31(5):358–61.

[35] Yang L, Zhang X, Liu S, Zhang W. Field test of large-scale hydrogen manufacturing from underground coal gasification. Int J Hydrogen Energy 2008;33:1275–85.
[36] Perkins G, Sahajwalla V. A numerical study of the effects of operating conditions and coal properties on cavity growth in underground coal gasification. Energy Fuels 2006;20:596–608.
[37] Stanczyk K, Smolinski A, Kapusta K, Wiatowski M, Swiadrowski J, Kotyrba A, et al. Dynamic experimental simulation of hydrogen oriented underground gasification of lignite. Fuel 2010;89:3307–14.
[38] Stanczyk K, Howaniec N, Smolinski A, Swiadrowski J, Kapusta K, Wiatowski M, et al. Gasification of lignite and hard coal with air and oxygen enriched air in a pilot scale ex situ reactor for underground gasification. Fuel 2011;90:1953–62.
[39] Stanczyk K, Kapusta K, Wiatowski M, Swiadrowski J, Smolinski A, Rogut J, et al. Experimental simulation of hard coal underground gasification for hydrogen production. Fuel 2011;91:40–50.
[40] Daggupati S, Ramesh N, Manadapati RN, Mahajani SM, Ganesh A, Mathur DK, et al. Laboratory studies on combustion cavity growth in lignite coal blocks in the context of underground coal gasification. Energy 2010;35:2374–86.
[41] Daggupati S, Ramesh N, Manadapati RN, Mahajani SM, Ganesh A, Chapru RK, et al. Laboratory studies on cavity growth and product gas composition in the context of underground coal gasification. Energy 2011;36:1776–84.
[42] Prabu V, Jayanti S. Laboratory scale studies on simulated underground coal gasification of high ash coals for carbon-neutral power generation. Energy 2012;46:351–8.
[43] Prabu V, Jayanti S. Simulation of cavity formation in underground coal gasification using bore-hole combustion experiments. Energy 2011;36:5854–64.
[44] Saulov D.N., Ovid A.P., Klimenko, A.Y. Flame propagation in a gasification channel, Energy 2010;35:1264–73.
[45] Wiatowski, M.; Stanczyk, K.; Swiądrowski, J.; Kapusta, K.; Cybulski, K.; Krause, E.; Grabowski, J.; Rogut, J.; Howaniec,N.; SmoliĔski, A. Semitechnical underground coal gasification (UCG) using the shaft method in Experimental Mine “Barbara.” Fuel 2012, 99, 170-179.
[46] Pei, P.; Nasah, J.; Solc, J.; Korom, S.; Laudal, D.; Barse, K.;. Investigation of the feasibility of underground coal gasification in North Dakota, United States, Energy Conversion and Management, 2016, 113, 95-103.
[47] Cui Yong, Liang Jie, Wang Zhangqing, Zhang Xiaochun, Fan Chenzi, Liang Dongyu, Wang Xuan. (2014). Forward and reverse combustion gasification of coal with production of high-quality syngas in a simulated pilot system for in situ gasification. Applied Energy, 131, pp.9-19.
[48] Blinderman M.S., Saulov D.N., Klimenko, A.Y. Flame propagation in a gasification channel. Energy 2010;35:1264–73.
[49] Wang FT, Mead SW, Stuermer DH, 1981, Groundwater contamination near the Hoe Creek UCG experiments. Lawrence Livermore National Laboratory: Livermore, CA, USA. UCRL-85880.
[50] Wang FT, Mead SW, Stuermer DH, 1982b, Mechanisms for groundwater contamination by UCG – Preliminary conclusions from the Hoe Creek Site. Lawrence Livermore National Laboratory: Livermore, CA, USA. UCRL-88012.

[51] Raber E, Stone R, 1980, Ground-water hydrologic effects resulting from underground coal gasification experiments at the Hoe Creek Site near Gillette, Wyoming. Lawrence Livermore National Laboratory: Livermore, CA, USA. UCID-18627.
[52] Lindblom SR, Smith VE. Rocky Mountain 1 underground coal gasification test, Hanna, Wyoming, groundwater evaluation. Technical Report DOE/MC/25038-36523, Western Research Institute: Laramie, WY, USA, 1993.
[53] Su F.Q., Itakura K, Deguchi G, Ohga K, Kaiho M. Evaluation of energy recovery from laboratory experiments and small-scale field tests of underground coal gasification (UCG). Journal of MMIJ 2015;131:203–18.
[54] Nakanowataru T., Su F.Q., Itakura K. Evaluation of crack extension inside the coal specimen under heating process, Spring Convention of the Mining and Materials Processing Institute of Japan, 2011 (Japan), A7-7, pp.187-188.
[55] Hardy Jr HR. Acoustic emission/microseismic activity: Principles, techniques and geotechnical applications. Vol 1, Taylor & Francis: Leiden, Netherlands; 2003.
[56] Hardy Jr HR. Source location velocity models for AE/MS field studies in geologic materials, In: Proceeding 3rd International Acoustic Emission Symposium, Tokyo, Japan, Japanese Society for Nondestructive Inspection, 1986. p. 365–88.
[57] Leighton F, Duvall WI. A least squares method for improving the source location of rock noise. U.S. Bureau of Mines, PI 7626, 1972.
[58] Ohtsu M. Simplified moment tensor analysis and unified decomposition of acoustic emission source: Application to in-situ hydrofracturing test. J Geophys Res 1991;1B:6211–21.
[59] Ohtsu M, Okamoto T, Yuyama S. Moment tensor analysis of acoustic emission for cracking mechanisms in concrete. ACI Struct J 1998;95:87–95.
[60] Kasahara K. Earthquake mechanics. Cambridge University Press; 1981; p. 92–102.
[61] Aki K, Richards PG. Quantitative seismology-theory and methods. Freeman (San Francisco) 1980;1:116–119.
[62] Ground motion-Its combined and waveform processing. Theoretical Earthquake Research, Kajima Institute Publishing Co., Ltd; 1994; p. 61–5.
[63] Ivanova V, Yu X, Veneziano D, Einstein H. Development of stochastic models for fracture systems. In: The 35th U.S. Symposium on Rock Mechanics (USRMS). American Rock Mechanics Association, 1995. p. 725–30.